Scripta Materialia 267 (2025) 116799

Contents lists available at ScienceDirect

Scripta Materialia

journal homepage: www.journals.elsevier.com/scripta-materialia

Retrokinetics of crystallization

Luke Hunter [a,b,*], Ryo Torii [c], Gaetano Burriesci [c,d,e], Sergio Bertazzo [a,f,*]

[a] Department of Medical Physics & Biomedical Engineering, University College London, London WC1E 6BT, UK
[b] Institute of Cardiovascular Science, University College London, London WC1E 6BT, UK
[c] Department of Mechanical Engineering, University College of London, London WC1E 6BT, UK
[d] Bioengineering Group, Ri.MED Foundation, Palermo 90133, Italy
[e] Department of Engineering, University of Palermo, Viale delle Scienze, 90128 Palermo, Italy
[f] London Centre for Nanotechnology, University College London, London WC1E 6BT, UK

ARTICLE INFO

Keywords:
Crystallization
Polycrystalline
Nucleation
Growth
Monte Carlo
Stochastic
Impinged

ABSTRACT

During crystallization, crystals nucleate and grow within materials, often impinging and interacting in a stochastic manner. This complexity has long hindered accurate reconstructions of a material's crystallization history. By considering a representative material region with a finite crystal population, we derive equations that accurately predict crystal size and free surface evolution throughout the crystallization process. These equations, paired with a numerical solver, enable reconstructing nucleation events and crystallinity progression using the crystal size distribution and growth rates. We demonstrate this method by pinpointing the nucleation and crystallinity timelines of simulated, manufactured, and ancient geological materials, entirely without real-time observation. Our model offers unprecedented insights into extreme crystallization environments that are difficult to mimic, such as volcanic magma chambers, and supports the design of advanced materials.

Introduction

Nucleation and growth are fundamental to how 2D [1–5] and 3D [5–7] materials form. Glass devitrification [1], electronic crystal formation [2], and ferroelectric domain growth [3] are all examples of transformations in materials where nuclei randomly appear and then grow, competing for space. The rate at which crystal nucleation and growth occur is particularly critical in determining how a material's structure develops. Predicting the nucleation rate of crystals is known to be a significant challenge, whereas predictions of crystal growth rates are often far more accurate [8,9]. Because predicting nucleation rates is challenging, their direct measurement is important to gain insights into crystallization. However, methods for measuring nucleation rates in materials are also limited. Direct observation of nuclei forming without disturbing their surroundings is challenging [5] and is impossible for materials that have already undergone crystallization.

In polycrystalline geological materials, determining the times of crystal formation provides crucial insights into the kinetics of geological processes, such as ore deposit formation [10] and lunar volcanic activity [11]. Current retrospective methods of measuring nucleation rates, which do not involve observation during the transformation, rely on measuring the crystal size distribution. These methods assume a specific functional form for the nucleation rate, a constant growth rate, and that crystal boundary impingement does not occur [11–14]. Recent works have identified improvements, enabling time-dependent growth rates to be independently determined. This is achieved by examining the partitioning of elements around crystal boundaries, a process referred to as 'geospeedometry' [15,16]. But methods to determine nucleation times still rely on the assumption of no impingement [15]. Despite this assumption, such techniques are often applied to materials that are near-fully crystalline because there is no accurate alternative [11,17].

The complexity of accounting for random crystal boundary impingements and the resulting distortion of the crystal morphology have hindered modelling crystallization. Empirical impingement corrections for models that retrospectively determine nucleation rates have been proposed [10,18]. However, their uncertain range of applicability has limited their widespread adoption. Whereas models of crystallization that rigorously account for impingement lack a method of retrospectively determining nucleation times of individual crystals [5,7,19–25]. These rigorous impingement models consider an infinitely large material with an infinite number of crystals forming within. We conjectured that deriving a model based on a finite number of crystals, instead of infinite, could enable predicting the size of individual crystals. Such a model could be used to accurately determine the nucleation rate in a

* Corresponding authors.
E-mail addresses: ucemlwh@ucl.ac.uk (L. Hunter), s.bertazzo@ucl.ac.uk (S. Bertazzo).

https://doi.org/10.1016/j.scriptamat.2025.116799
Received 26 February 2025; Received in revised form 27 May 2025; Accepted 28 May 2025

material that was not observed during crystallization.

Most models of crystallization under impingement, like the Avrami equation [19–23] which is often applied to materials transformations [1–7], assume crystals nucleate randomly throughout an infinite space and grow until their boundaries reach another's. The parts of the boundary that meet cease moving. Nucleation and growth continue until the whole system is occupied.

We instead considered an arbitrary region of a material. This region is finite and has periodic boundaries. If crystals nucleate randomly within uncrystallized space in the region and then grow, we find that their expected combined volume fraction, individual volume fraction, and unimpinged free surface area over time are given by Eqns. S7, S9, and S11 (see Supplementary Information for derivation). If nuclei form at different times, then Eqns. S7, S9, and S11 predict that each crystal will have a different size and free surface, creating a distribution of crystal sizes and free surfaces.

To validate our theoretical predictions, we tested the accuracy of the predicted distributions of Eqns. S7, S9, and S11 against 2D and 3D simulations for various nucleation and growth scenarios. Three scenarios representative of many material transformations were considered: 1) constant nucleation and growth rate in 2D [2,4,7], 2) constant nucleation rate and time-dependent growth rate in 2D [1,7], 3)

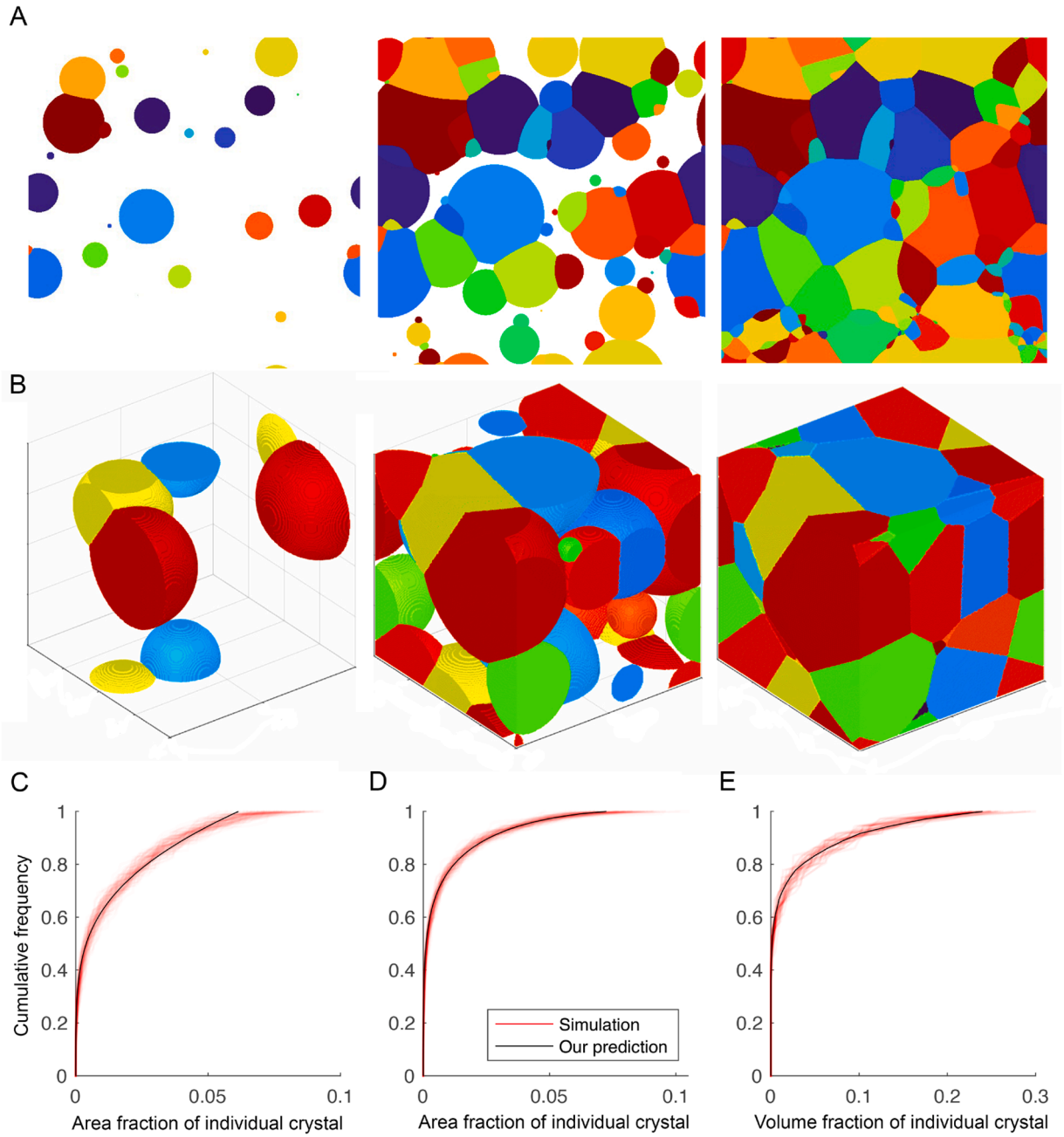

Fig. 1. Comparison of our equations' predictions to simulations. Representative timelapse snapshots of simulations early, midway, and at the end of crystallization in 2D (A) and 3D (B). (C-E) Cumulative frequency distribution diagrams illustrating the similarity between the predicted and simulated final crystal size distributions in each scenario. Each red line corresponds to the result of one Monte Carlo simulation run. The exact scenarios are scenario 1 (C): nucleation rate $= 0.5\ s^{-1}$, radial growth rate 1 pixel s^{-1}; scenario 2 (D): nucleation rate $= 0.5\ s^{-1}$, radial growth rate $\frac{5}{\sqrt{t}}$ pixels s^{-1} where t is time since experiment began such that all crystals grow at the same rate; scenario 3 (E): nucleation rate $= 0.005t\ s^{-1}$, where extended radii are given by $\sqrt{120(t - t_{n,i})}$ voxels where $t_{n,i}$ is time of crystal i's nucleation, such that the extended radius of crystal i is proportional to the time elapsed, $(t - t_{n,i})$, since its nucleation.

time-dependent nucleation rate and parabolic growth rate in 3D [8]. Monte Carlo cellular automata simulations were performed using Matlab (Mathworks, USA). Crystal nuclei, one pixel or voxel in size, were randomly initiated in unoccupied regions of a square or cubic domain at times dictated by the prescribed nucleation rate. Volume and area fractions (for individual crystals and the overall phase) were determined via voxel or pixel counting, while surface area and perimeter were measured using the line intercept count method [26]. For the 3D simulations, the line intercept count was sampled on 20 equally spaced planes along the cube's depth. In 2D, 100 independent simulations were conducted using a central grid of 600^2 (with a total grid of 1800^2 when accounting for periodic boundaries) to determine mean crystal sizes, free surfaces, and distribution characteristics. For 3D, due to higher computational demands, 40 independent simulations were performed using a central grid of 200^3 (total grid of 600^3 when including periodic boundaries) to obtain the corresponding measurements.

Characteristic timelapse images of the 2D and 3D simulations are shown in Fig. 1A and B. Our equations accurately predicted the crystal size distributions at the end of each simulated crystallization scenario (Fig. 1C-E). Deviations between simulation results and theoretical predictions (Eqns. S7, S9, and S11) for crystal size and free surface distributions at different transformation stages are summarized in Table 1 and shown in Fig. S1-S2.

Predicting the crystal size distribution during crystallization could be very useful for designing materials with bespoke properties. Many electrical, mechanical, and antimicrobial properties of polycrystalline materials depend on the crystal sizes and free surfaces [27–29]. Our equations illustrate the dominant factors that determine these crystal sizes and free surfaces. Multiple scenarios can be computed in seconds on a laptop. Whereas random-seed simulations, which require taking averages of multiple runs, can take days to complete a single scenario. Thus, our equations offer a tool to rapidly evaluate advanced material production strategies via processing-structure-property relationships [27].

As with the Avrami equation, our model assumes nuclei remain spatially fixed during growth. This may be a reasonable approximation in some fluid systems [1,6,28] but general application to crystallization in fluid media requires caution as crystal movement can occur in the media via convection or settling.

To our knowledge, there are no models of finite materials for predicting crystal sizes or free surfaces under the effect of impingement. Recent work has identified a method for predicting the crystal size distribution in infinite materials via Fokker-Planck equations [24,25]. However, these require defining functional forms of the nucleation and growth rate that apply to every crystal. Our method instead treats crystals individually, so nucleation times and growth rates for individual crystals can be specified, giving granular control over the model.

Eqns. S7 and S9 showed that the final volume of each crystal is dependent on the history of the system, including the effects of all other crystals. This led us to develop a system of equations whereby, if either the nucleation or growth rate is known, the other can be determined from the measured crystal size distribution.

We extended Eqns. S7 and S9 to account for not all crystals having boundaries fully within an imaged region, which yielded Eqns. S13–15, and developed a numerical solver in Matlab that would optimize a set of equations to best match a measured crystal size distribution (see Supplementary Information for full derivation).

$$KV_{Vi,measured} = \int_0^{\tau} \frac{d\left(KV_{Vi,extended}\right)}{dt} \frac{\left(1 - KV_{Vi,extended}\right)\left(1 - KV_{Vj,extended}\right)\cdots}{\left(1 - KV_{Vi,extended}\right)} dt$$

$$KV_{Vj,measured} = \int_0^{\tau} \frac{d\left(KV_{Vj,extended}\right)}{dt} \frac{\left(1 - KV_{Vi,extended}\right)\left(1 - KV_{Vj,extended}\right)\cdots}{\left(1 - KV_{Vj,extended}\right)} dt$$

Where $V_{Vi,measured}$ is the measured area or volume fraction of an individual crystal which can be found via many methods such as stereology and X-ray tomography [11,15,26]. K is a constant found by dividing the area or volume fraction of all crystals by the sum of crystal area or volume fractions that are fully within the imaged region. $V_{Vi,extended}$ is the 'extended' area or volume fraction [21–23] of an individual crystal and defines the area or volume fraction the crystal would have if it didn't impinge on any other crystal. τ is the desired experiment end time. There is an equation for each crystal in the system, so if there are n crystals measured then there are a set of n equations. When the growth rate is not a function of time since the experiment began, such as for constant or parabolic growth, the nucleation time of the first crystal (which is expected to be the largest according to Eqn. S15) is set to zero to provide a fixed reference point for the optimization. When the growth rate is a function of time since the experiment began, such as growth dependent on the rate a material is cooled, no other reference point is required and the times of nucleation can be given in terms of time since the experiment began. We also state that no crystal can form earlier than $t = 0$ or later than the measured end time of the experiment. Alternatively, if any crystal's extended area fraction will reach unity before the measured end time then this is taken as the end time. If this step is not done, Eqn. S14 becomes negative.

We tested the ability of our method to reconstruct the nucleation times given the crystal size distribution predicted by Eqns. S7 and S9 from the scenarios in Fig. 1. The inputs were the known experiment time, final crystal size distribution, and the prescribed growth rate. In each scenario, the nucleation rates were accurately determined (Fig. 2).

We then applied our method to an evaporative crystallization experiment, the most common industrial crystallization method [30]. We used the prototypical system of spherulitic ascorbic acid crystals [31]. Spherulites are a crystal morphology resembling circles in 2D and spheres in 3D. They are likely the most widespread crystal morphology [32] and occur in many materials, from metal to magma [1,2,4–8,15,16,32,33]. 2 ml of a 0.032 g/ml solution of ascorbic acid in methanol (Sigma-Aldrich, UK) was pipetted into fresh 9 cm diameter plastic evaporation dishes over a lightbox. Crystallization of a central square region of each dish, away from the dish edges, was monitored with timelapse images taken using a Canon EOS 5D Mark IV (Canon, Japan). Throughout crystallization, a temperature of 24°C and a humidity of 33–37 % was maintained. Nucleation times were taken to be the times that new crystals were first visible in the timelapse images. Area fraction and perimeter measurements were made using the point counting and line intercept methods [26]. The measured area fractions of crystals fully within the central square region, experiment end times, and central square region sizes are given in Table S1.

Timelapse images show the progress of crystallization (Fig. 3A-C) and the ascorbic acid crystals produced structures typical of concurrent

Table 1
Summary statistics of percentage difference between predictions of Eqns. S7, S9, and S11 against simulation results.

Crystallization Stage	Crystal property	Scenario 1 (%)	Scenario 2 (%)	Scenario 3 (%)	Average (%)
Early in transformation	Size distribution	2.1	1.2	2.3	1.85
	Free surface distribution	3.7	3.8	2.7	3.4
Midpoint	Size distribution	2.6	2	2.4	2.3
	Free surface distribution	6.3	4	7.6	6
End of transformation	Size distribution	2	1.2	1.3	1.5

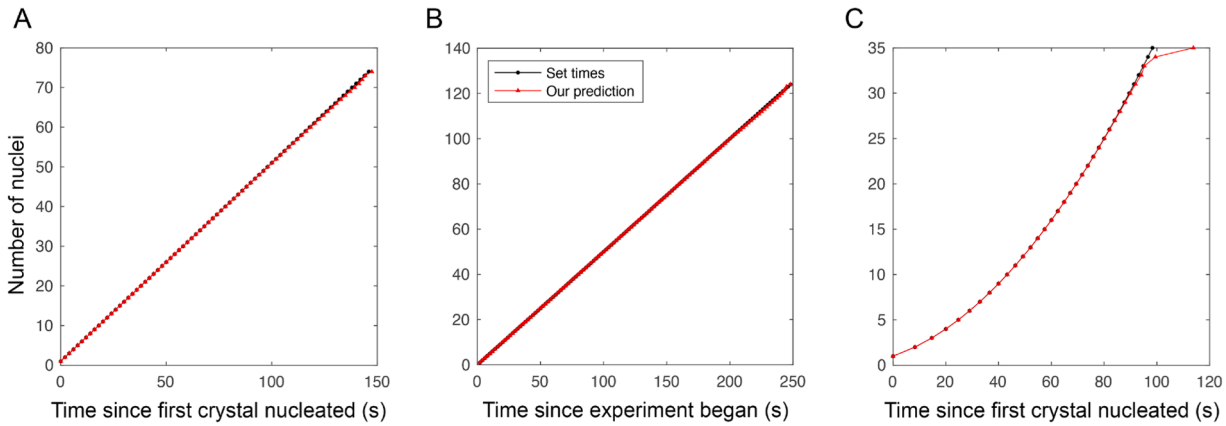

Fig. 2. Reconstructed times of crystal nucleation from nucleation and growth scenarios. Plots of prescribed number of nuclei over time in (A) scenario 1, (B) scenario 2, (C) scenario 3, vs. our reconstruction.

nucleation and growth (Fig. 3C cf. Fig. 1A). Contiguity is the ratio of non-free surface to total surface of the crystals [34] and is sensitive to the spatial randomness of nuclei but insensitive to their shape, nucleation rate, and growth rate in 2D and 3D [35]. A shallow deviation from a line of contiguity = combined crystal fraction that is most prominent mid-transformation is typical of spatially random nucleation [35]. The measured contiguity of the ascorbic acid crystals corresponded well to that expected of random nucleation (Fig. 3D). The histograms of measured final crystal sizes approximately correspond to a gamma distribution (Fig. 3E), as expected of random nucleation and growth of spherulites [24,25].

Our experiment used a density of 1 mg/cm^2 ascorbic acid over the evaporation dish. Previous work has shown that at this density, crystals grow at a constant rate of 3.5 μm/s [33]. We measured our crystal growth rates and they remained approximately constant at 3.5 μm/s over time (Fig. S3).

We then applied our model. The inputs were the predicted growth rate [33], our measured final crystal size distribution (of crystals fully within the field of view), and the total time of the experiment. The predicted times of crystal nucleation accurately match the measured times (Fig. 3F-G). The average error over time of the predictions was 2 nuclei (sample 1: 3, sample 2: 2), equivalent to an average percentage error of 7.2 % (sample 1: 8 %, sample 2: 6.4 %), and our predictions captured the qualitative change in nucleation behavior over time well. The observed nucleation profiles are typical of nucleation in materials with an initial slow increase, followed by a region of near-constant nucleation, then a slow plateauing [36].

The generalized Avrami equation [7,21–23] fit well to our data and the recovered exponent had an average value of 3.34 (Sample 1: 3.38, Sample 2: 3.29) (Fig. S4). However, these fractional exponents have no clear physical interpretation [7]. Hence, the Avrami exponent method of interrogating nucleation kinetics appears less generally applicable than our method, even in simple systems.

We then checked if our method could retrospectively predict other useful features of the crystallization process. One commonly sought metric is the combined crystallinity of the sample over time [1–8]. We used our predictions of nucleation times (Fig. 3F-G), the predicted growth rate [33], and Eqn. S7 to retrospectively predict the crystallinity of the sample over time. Our prediction matched the measured data well (Fig. 3H-I). To our knowledge, no other technique can pinpoint nucleation times or other crystallization properties, in systems that impinge, from data obtained after crystallization finishes.

We next applied our method to two datasets of crystals from obsidian lava samples taken from the caldera around Yellowstone supervolcano [15] (Fig. 4A). After eruptions around 100 million years ago [37], lava from the volcano slowed, cooled, and became highly viscous [15,16]. Crystals then began to randomly nucleate and grew until impingement [15,16]. Crystal formation is believed to have occurred whilst the lava was cooling from 600 to 350°C [15] (Fig. 4B). We plotted predicted nucleation times for a representative set of crystals from both datasets (Fig. 4C). These standard predictions were determined by assuming impingement did not occur. Then we applied our method. The inputs were the crystal size distribution, the time-dependent growth rate, and the crystallization time window. Large optimization problems can be computationally intensive and only ~70 crystals are needed for a representative sample element of a polycrystalline material [11], hence we sampled 70 crystals from the size distributions in the datasets [15]. The Matlab code used to compute the representative example of sample 1 in Fig. 4C has been deposited in the Supplementary Materials.

Our results suggested that some crystals nucleated nearly a year later than previously believed whilst others formed earlier (Fig. 4C). These observations reflect the changing availability of free space as crystallization proceeds. Early-nucleating crystals grow into relatively open regions and can grow unhindered, whereas later-nucleating crystals must grow into a more crowded space. As a result, to reach a given final size under tighter spatial constraints, a crystal must nucleate sooner. Crystals that nucleate later end up smaller because they grow in this more confined space.

The difference between our prediction and the standard prediction is clearest in sample 2 (Fig. 4C). Our method predicts that 26 % of the crystals nucleated 50 % later than the standard prediction. This suggests a secondary peak in nucleation rate, which can occur during the cooling of lava [15]. Our prediction illustrates the impact that accounting for impingement can have on determining the kinetics of geological processes.

Our derived equations accurately predict crystal size and free surface evolution during crystallization, accounting for impingement. Unlike random-seed Monte Carlo simulations, which require days to complete a single scenario through averaging multiple runs, our method enables the rapid evaluation of advanced material production strategies through informing processing-structure-property relationships [27]. We further found that these equations, combined with measurements of the crystal size distribution and predicted growth rate, can determine the times that individual crystals nucleated to a high accuracy of ±2 nuclei (or ±7.2 %) over the entire transformation, without any real-time observation required. Our method has broad implications in materials science and geology and could unravel the kinetics of crystallization in difficult-to-mimic extreme environments, such as magma chambers [11,14], while also informing the design of advanced materials like metastable cryogenic liquids, that resist ice formation, for organ preservation [6].

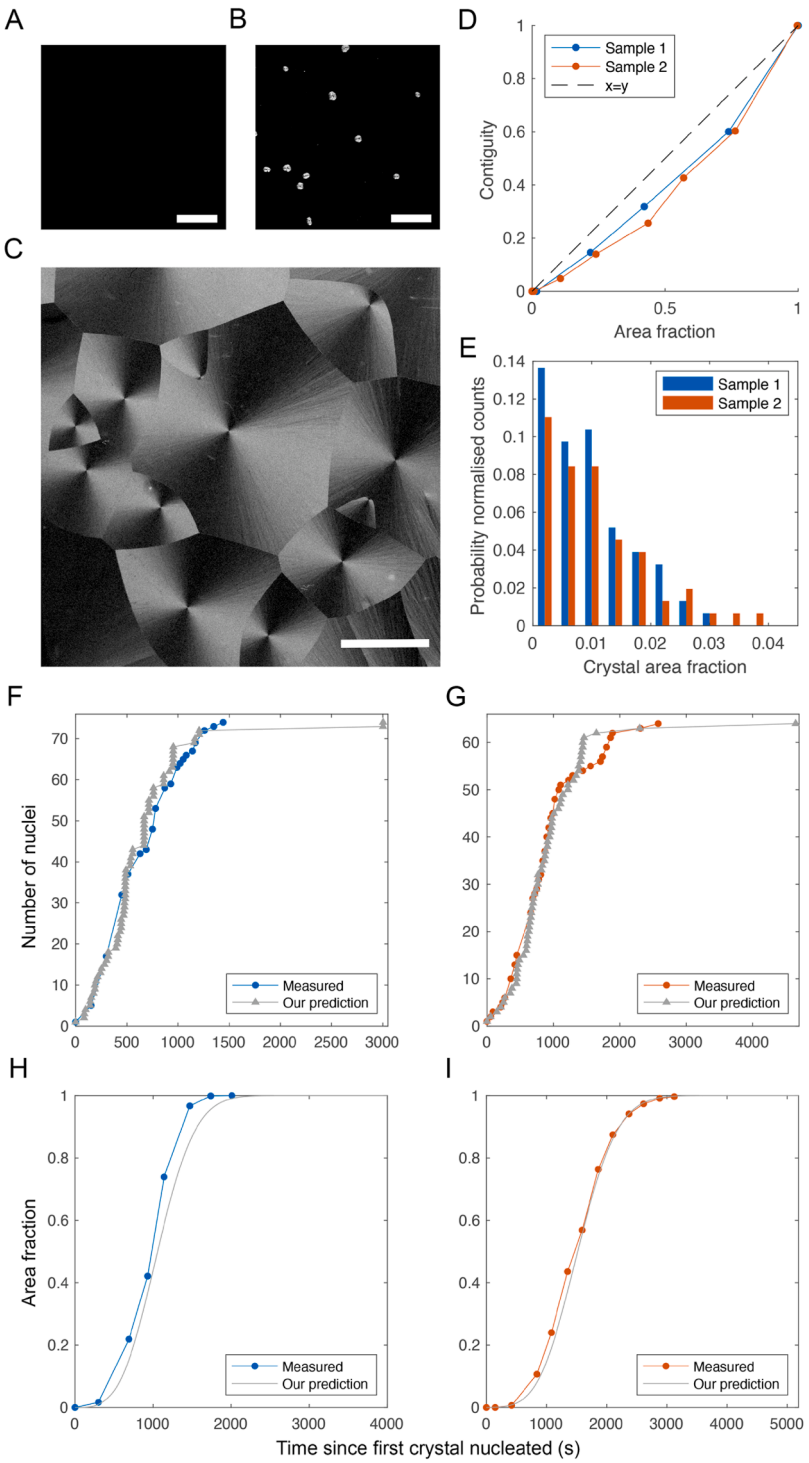

Fig. 3. Retrospective predictions on the kinetics of ascorbic acid evaporative crystallization. (A-C) Representative images of the progress of nucleation and growth of ascorbic acid crystals, scale bar is 4.5 mm in all pictures. (D) Contiguity of each sample vs. combined crystal area fraction. (E) Histogram of probability normalized crystal area fractions for each sample at the end of crystallization. Measured and retrospective predictions of nucleation rate for: (F) sample 1 and (G) sample 2. Measured and retrospective predictions of combined crystal area fraction over time for: (H) sample 1 and (I) sample 2.

Funding

British Heart Foundation grant FS/4yPhD/F/20/34134 (LH).

CRediT authorship contribution statement

Luke Hunter: Writing – review & editing, Writing – original draft, Visualization, Validation, Software, Resources, Methodology, Investigation, Funding acquisition, Formal analysis, Data curation, Conceptualization. **Ryo Torii:** Writing – review & editing, Supervision. **Gaetano Burriesci:** Writing – review & editing, Supervision. **Sergio Bertazzo:** Writing – review & editing, Supervision, Methodology.

Declaration of competing interest

The authors declare that they have no known competing financial

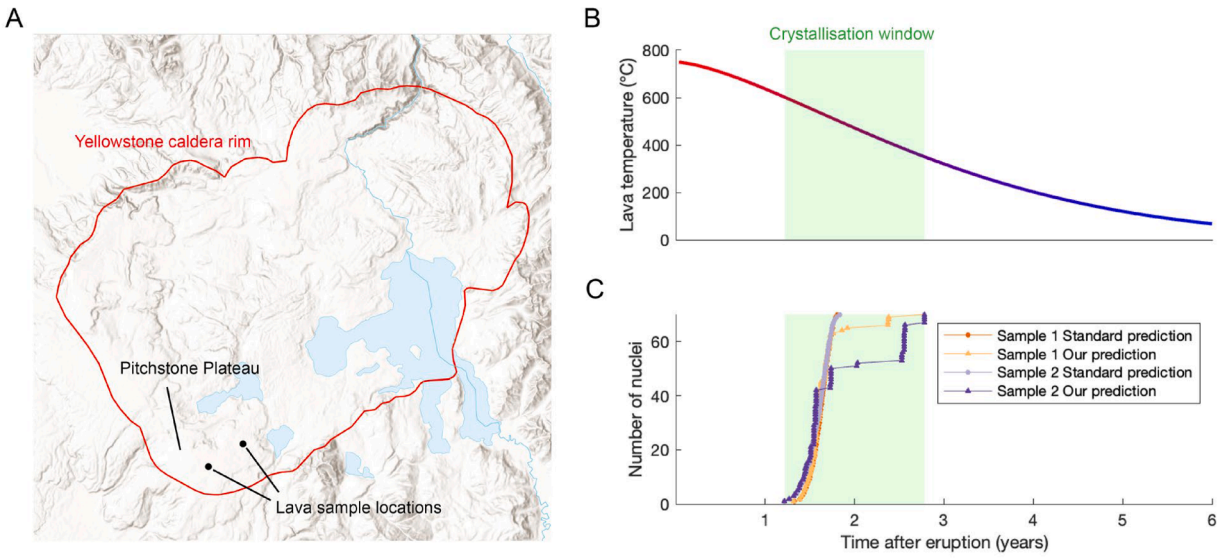

Fig. 4. Retrospective kinetics of geological crystallization. (A) Map of Yellowstone supervolcano with the approximate position of the caldera rim highlighted [38]. The datasets, Y22 and Y193, are from two locations in the Pitchstone Plateau lava field [15]. We only considered datasets Y22 and Y193 from the Pitchstone Plateau lava field as Gardner et al. [15] note stronger supporting evidence for their crystal growth rate determinations. (B) Proposed temperature profile of lava cooling with the 600 to 350°C crystallization window highlighted [15]. (C) Nucleation times of a representative set of 70 crystals sampled from each dataset predicted using the standard method vs. our method. Map source credits: Esri, CGIAR, USGS, TomTom, Garmin, SafeGraph, FAO, METI/NASA, Bureau of Land Management, EPA, NPS, USFWS.

interests or personal relationships that could have appeared to influence the work reported in this paper.

Supplementary materials

Supplementary material associated with this article can be found, in the online version, at doi:10.1016/j.scriptamat.2025.116799.

References

[1] C. Herrero, et al., Two-step devitrification of ultrastable glasses, Proc. Natl. Acad. Sci. 120 (16) (2023) e2220824120.
[2] T. Sato, K. Miyagawa, K. Kanoda, Electronic crystal growth, Science 357 (6358) (2017) 1378–1381.
[3] S. Liu, I. Grinberg, A.M. Rappe, Intrinsic ferroelectric switching from first principles, Nature 534 (7607) (2016) 360–363.
[4] Y. Ahn, et al., X-ray nanodiffraction imaging reveals distinct nanoscopic dynamics of an ultrafast phase transition, Proc. Natl. Acad. Sci. 119 (19) (2022) e2118597119.
[5] K. Kelton, A.L. Greer, Nucleation in Condensed Matter: Applications in Materials and Biology, 1st ed., Elsevier, Oxford, UK, 2010.
[6] C. Alba-Simionesco, et al., Interplay of vitrification and ice formation in a cryoprotectant aqueous solution at low temperature, Proc. Natl. Acad. Sci. 119 (12) (2022) e2112248119.
[7] Q. Zheng, et al., Understanding glass through differential scanning calorimetry, Chem. Rev. 119 (13) (2019) 7848–7939.
[8] S.E. Offerman, et al., Grain nucleation and growth during phase transformations, Science 298 (5595) (2002) 1003–1005.
[9] D. Erdemir, A.Y. Lee, A.S. Myerson, Crystal nucleation, in: A.Y. Lee, A.S. Myerson, D. Erdemir (Eds.), Handbook of Industrial Crystallization, Cambridge University Press, Cambridge, 2019, pp. 76–114. Editors.
[10] A.C. Lasaga, Kinetic Theory in the Earth Sciences, Princeton University Press, Princeton, 1998.
[11] B. Luo, et al., The magmatic architecture and evolution of the Chang'e-5 lunar basalts, Nat Geosci 16 (4) (2023) 301–308.
[12] B.D. Marsh, Crystal size distribution (CSD) in rocks and the kinetics and dynamics of crystallization, Contributions Mineral. Petrol. 99 (3) (1988) 277–291.
[13] K.V. Cashman, B.D. Marsh, Crystal size distribution (CSD) in rocks and the kinetics and dynamics of crystallization II: Makaopuhi lava lake, Contributions Mineral. Petrol. 99 (3) (1988) 292–305.
[14] K.V. Cashman, Crystal size distribution (CSD) analysis of volcanic samples: advances and challenges, Front. Earth Sci. 8 (2020).
[15] J.E. Gardner, et al., Nucleation rates of spherulites in natural rhyolitic lava, Am. Mineral. 101 (11) (2016) 2367–2376.
[16] K.S. Befus, et al., Spherulites as in-situ recorders of thermal history in lava flows, Geology 43 (7) (2015) 647–650.
[17] H.-C. Tian, et al., Non-KREEP origin for Chang'e-5 basalts in the Procellarum KREEP Terrane, Nature 600 (7887) (2021) 59–63.
[18] V. Špillar, D. DolejŠ, Calculation of time-dependent nucleation and growth rates from quantitative textural data: inversion of crystal size distribution, J. Petrol. 54 (5) (2013) 913–931.
[19] Kolmogorov, A.N., On the Statistical Theory of Crystallization of Metals [in Russian]. Izv. Akad. Nauk SSSR, 1937. Ser. Mat.(3): p. 355–359.
[20] W. Johnson, R. Mehl, Reaction kinetics in processes of nucleation and growth, Trans. Metall. Soc. AIME 135 (1939) 416–442.
[21] M. Avrami, Kinetics of phase change. I General theory, J Chem. Phys. 7 (12) (1939) 1103–1112.
[22] M. Avrami, Kinetics of phase change. II transformation-time relations for random distribution of nuclei, J. Chem. Phys. 8 (2) (1940) 212–224.
[23] M. Avrami, Kinetics of phase change. III granulation, phase change, and microstructure, J Chem Phys 9 (2) (1941) 177–184.
[24] M. Tomellini, On the grain size distribution function in KJMA compliant growth, J. Cryst. Growth 584 (2022) 126579.
[25] M. Tomellini, Fokker–Planck equation for the particle size distribution function in KJMA transformations, Physica A Stat. Mech. Appl. 615 (2023) 128515.
[26] J.C. Russ, R.T. Dehoff, Practical Stereology, Springer Science & Business Media, 2000.
[27] G.B. Olson, Computational design of hierarchically structured materials, Science 277 (5330) (1997) 1237–1242.
[28] W. Haller, Rearrangement kinetics of the liquid—Liquid immiscible microphases in alkali borosilicate melts, J. Chem. Phys. 42 (2) (1965) 686–693.
[29] L. Wondraczek, et al., Artificial microbial arenas: materials for observing and manipulating microbial consortia, Adv. Mater. 31 (24) (2019) 1900284.
[30] H.J.M. Kramer, R. Lakerveld, in: A.Y. Lee, A.S. Myerson, D. Erdemir (Eds.), Selection and Design of Industrial Crystallizers, in Handbook of Industrial Crystallization, Cambridge University Press, Cambridge, 2019, pp. 197–215. Editors.
[31] P. Ball, Patterns in Nature: Why the Natural World Looks the Way It Does, University of Chicago Press, 2016.
[32] A.G. Shtukenberg, et al., Spherulites, Chem. Rev. 112 (3) (2012) 1805–1838.
[33] Y. Yamazaki, et al., Existence of thickness threshold for crystal growth rate of ascorbic acid from its thin solution film, J. Cryst. Growth 468 (2017) 43–45.
[34] J. Gurland, The measurement of grain contiguity in two-phase alloys, Trans. Metall. Soc. AIME 212 (1958) 452–455.
[35] R.B. Godiksen, et al., Three-dimensional geometric simulations of random anisotropic growth during transformation phenomena, Scr. Mater. 58 (4) (2008) 279–282.
[36] R.W. Balluffi, S.M. Allen, W.C. Carter, Kinetics of Materials, John Wiley & Sons, Hoboken, NJ, 2005.
[37] R.L. Christiansen, et al., Preliminary Assessment of Volcanic and Hydrothermal Hazards in Yellowstone National Park and Vicinity, U. S. Geological Survey, 2007.
[38] R.L. Christiansen, The Quaternary and Pliocene Yellowstone Plateau Volcanic Field of Wyoming, Idaho, and Montana, US Geological Survey, 2001.